Performance of Immobilized Photocatalytic Reactors in Continuous Mode

M. F. J. Dijkstra, E. C. B. Koerts, A. A. C. M. Beenackers, and J. A. Wesselingh
University of Groningen, Dept. of Chemical Engineering, Nijenborgh 4, 9747 AG, Groningen, The Netherlands

A packed-bed (PBR), fiber (FR), membrane (MR), and tubular (TR) photocatalytic reactor have been modeled to compare their performance on a pilot scale. The influence of radial dispersion in the PBR and mass-transfer limitation in the PBR, FR, and TR has been taken into account. The oxygen concentration in the liquid has a large influence on the performance and, therefore, air or pure oxygen should be added. The MR and PBR have a better performance than the TR and FR. Only a small degree of mass-transfer limitation occurs in the PBR. Radial dispersion hardly influences the performance of the PBR. External mass-transfer limitation influences the conversion in the TR and FR severely. The PBR, MR, and TR show a much better energy efficiency than the FR.

Introduction

Like other advanced oxidation technologies (AOTs), heterogeneous photocatalysis is an emerging technology for water purification. Almost any organic pollutant present in water can totally be degraded to carbon dioxide, water, and mineral acids. Heterogeneous photocatalysis for water purification is based on a semiconductor, usually TiO_2, and UV-A radiation (< 385 nm). The light activates the semiconductor by generating electron–hole pairs. These charge carriers can participate in redox reactions at the surface and form hydroxyl radicals, which can degrade the pollutant (Halmann, 1996; Hoffmann et al., 1995; Mills et al., 1997; Bahnemann, 1999; Serpone and Pellizetti, 1989; Schiavello, 1997).

In the field of heterogeneous photocatalysis, much research has been performed on the laboratory scale, but no industrial application exists to our knowledge. One of the reasons that prevented this technology from being established in industrial installations is the absence of efficient reactors, proper reactor design, and reactor optimization (Ollis et al., 1991; Legrini et al., 1993; Rajeshwar, 1995; Maurino et al., 1999).

Reactors presented in the literature can be divided into two categories: reactors using solar light, and those using artificial light. The solar reactors will not be discussed, since our project focuses on reactors using artificial light. A summary of the most important reactor designs in the artificial-light reactor category is given in Table 1.

Slurry reactors have often been investigated (Cassano et al., 1995): in the laboratory, an immersed annular reactor is the type most used. A promising design is that using a thin flowing film of a titanium dioxide suspension over an illuminated glass plate or annulus (Ollis and Turchi, 1990; Yue, 1997). The cocurrent downflow contactor reactor has two sections. In the top part, the pollutants adsorb onto the catalyst; in the lower part the slurry is irradiated to degrade the pollutants (Winterbottom et al., 1997). Several designs are meant to enhance the mixing of the suspension so that all of the catalyst can be illuminated (for example, by using a rotating glass tube) (Karpel Vel Leitner et al., 1996; Sczechowski et al., 1995; Fabiyi and Skelton, 1999; Lea and Adesina, 1999; Sobczyński et al., 1997).

In reactors with an immobilized catalyst, the utilization of light is improved by optical fibers coated with titanium dioxide that transmit the light (Marigangeli and Ollis, 1980; Hofstadler et al., 1994; Peill and Hoffmann, 1996). In fluidized- and packed-bed photocatalytic reactors, a large specific area is created using titanium dioxide coated on silica-based carriers or titanium dioxide pellets (Dijkstra et al., 2001; Al-Ekabi and Serpone, 1988; Raupp et al., 1997; Zhang et al., 1994; Sclafani et al., 1993; Yamazali-Nishida et al., 1993; Starosud et al., 1999; Dibble and Raupp, 1992; Haarstrick et al., 1996; Pozzo et al., 1999). Bellobono et al. developed a reactor in which three membranes with TiO_2 were annularly placed

Correspondence concerning this article should be addressed to. M. F. J. Dijkstra.

around a tube light (Bellobono et al., 1998). Ray and Beenackers (1998a) developed a reactor that consists of ultrathin tubes (diameter of 4 mm) coated with catalyst. The tubular reactor is a reactor in which wastewater flows through two concentric glass tubes: the inner tube is coated with catalyst and contains the UV tube (Dijkstra et al., 2001). Another type of tubular reactor is the coated-wall reactor (Mazzorino and Piccinini, 1999; Mazzorino et al., 1999). In this reactor, the liquid flows between the coated tube and the UV tube.

In this work, the performances of several reactors are compared to better understand their limitations and advantages. Of the ones just mentioned, the following reactors are chosen:

- Packed-bed reactor (PBR)
- Tubular reactor (TR)
- Membrane reactor (MR)
- Fiber reactor (FR).

The reactors that use a suspended nanocatalyst have the disadvantage that they require catalyst separation. Therefore, they are not considered in this study. The fluidized-bed reactor is not considered, because we have not been able to obtain wear-resistant catalyst layers. The reactor with the ultrathin tube lights was not chosen, because the lamps have stability problems, nor was the coated-wall reactor taken into account.

In the photocatalytic reactors that have been selected, the following aspects are considered:

- Catalyst loading
- Influence of internal and external mass-transfer limitation
- Presence of a third gas phase (air or oxygen)
- Variations of the liquid and gas flow rates.

In the PBR the radial profile was taken into account. The performance in a continuous mode is modeled for the photocatalytic degradation of formic acid (FA) with kinetic models developed in previous work (Dijkstra et al., 2002; Dijkstra, 2002). Conclusions from this theoretical comparison with an eye to the reactor design are drawn.

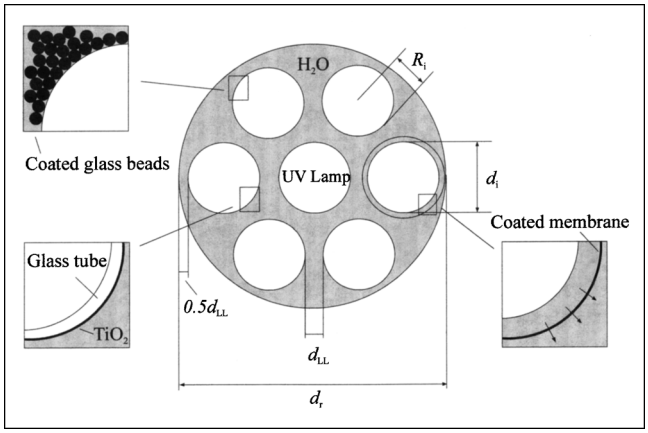

Figure 1. Packed bed, membrane, and tubular reactors.

Photocatalytic Reactor Configurations

The PBR, TR, and MR have the seven-tube configuration shown in Figure 1. This can be used as a module for larger plants. Each glass tube contains a standard UV lamp; process water flows upwards along the tubes. In the MR, the liquid is forced to flow through the membrane by introducing the liquid in the gap between the glass tube and the membrane. In many cases, a gas stream, which also flows upwards, is applied. In the FR of Figure 2, there are no tubes. Instead,

Table 1. Literature Overview of Reactor Configurations (Artificial Illumination)

Catalyst Configuration	Reactor Type	Ref.
Slurry	Immersion-type annular reactor	Halmann (1996)
	Thin-film reactor	Ollis and Turchi (1990); Yue (1997); Puma and Yue (1998a,b; 1999)
	Cocurrent downflow contactor reactor (CDCR)	Winterbottom et al. (1997); Boyes et al. (1997)
	Rotating tube (Couette–Taylor flow)	Karpel Vel Leitner et al. (1996); Sczechowski et al. (1995)
	Bubble column	Lea and Adesina (1999)
	Pulsed-baffle tube photochemical reactor	Fabiyi and Skelton (1999)
	Air-lift loop photoreactor	Sobczyński et al. (1997)
	Fountain reactor	Puma and Yue (2000)
Immobilized	Fiber reactor	Marigangeli and Ollis (1980); Hofstadler et al. (1994); Peill and Hoffmann (1995, 1996)
	Ultrathin UV-tube lamps	Ray and Beenackers (1998a)
	Hollow-tube lamps	Ray and Beenackers (1998b); Ray (1999)
	Coated-wall reactor	Mazzarino and Piccini (1999); Mazzarino et al. (1999)
	Packed-bed reactor	Dijkstra et al. (2001); Al-Ekabi and Serpone (1988); Raupp et al., (1997) Zhang et al. (1994); Sclafani et al. (1993); Yamazali-Nishida et al. (1993)
	Fluidized-bed reactor	Starosud et al. (1999); Dibble and Raupp (1992); Haarstrick et al. (1996); Pozzo et al. (1999)
	Honeycomb monolithic reactor (air purification)	Hossain et al. (1999); Sauer and Ollis (1994)
	Membrane reactor	Bellobono et al. (1995, 1997, and 1998); Gianturco and Vianelli (1996)
	Glass-mesh reactor	Matthews (1993); Serrano and de Lasa (1997, 1999); Topudurti et al. (1998)
	Rotating disk reactor	Dionysiou et al. (2000)
	Coated tube reactor	Dijkstra et al. (2001); Al-Ekabi and Serpone (1988); Matthews (1988)

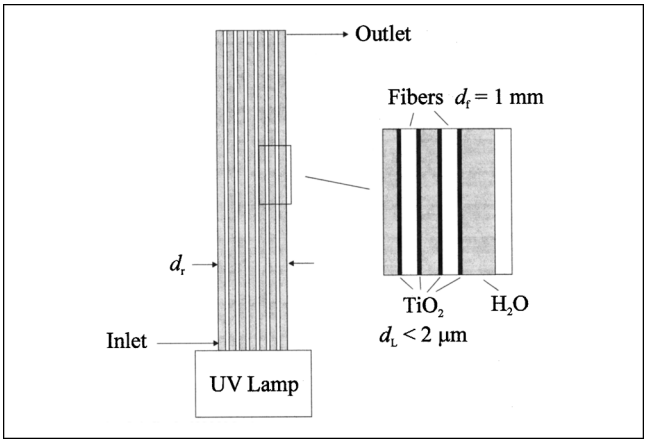

Figure 2. Fiber reactor.

light is carried into the liquid by a large number of fibers. It is assumed that the light input is the same as that in the other designs. The dimensions of the reactors are given in Table 2.

The catalyst is a thin film of TiO_2 particles with a thickness that is smaller than 3 μm. In the PBR, the catalyst is on the surface of the spherical particles used in the packed bed; here the catalyst loading has been varied between 0.5 and 4 $g \cdot m^{-2}$ (Dijkstra et al., 2001). The catalyst in the TR is applied as a film on the tubes, with a loading between 0.5 and 2 $g \cdot m^{-2}$ ($d_L = 0.3$–1.3 μm) (Dijkstra et al., 2002). In the MR the catalyst film on the membrane has a loading of 2 $g \cdot m^{-2}$. This is lower than that used in the study by Bellobono et al. (1995), which we have used as a starting point, because calculations showed that most of the light was absorbed in a very small part of the membrane. The catalyst in the FR, which is a similar film to that on the tubes, also has a loading of 2 $g \cdot m^{-2}$ ($d_L = 1.3$ μm).

The particles in the PBR have a diameter of either 1.3 or 2 mm. The porosity of the particle layer is assumed to be equal to that measured in the lab reactor [0.37 for the 1.3-mm particles and 0.42 for the 2-mm particles (Dijkstra, 2002)]. In the MR the membrane is cylindrical, with an inner diameter of 64 mm; the thickness is equal to that of the membrane of Bellobono et al. (1995), 1 mm. It has not been optimized for pressure drop over the membrane. The fibers in the FR have a thickness of 1 mm; we have considered modules with 2,170 fibers [porosity of reactor is 0.94 (Peill and Hoffmann, 1998)] and 4,340 fibers each. The length of the fibers is 0.7 m, which is equal to the illuminated length. The volume of the FR is equal to that of the other reactors.

Table 2. Configuration and Process Parameters of Different Reactors

	PBR, MR, TR	FR
d_i [m]	58×10^{-3}	
d_r [m]	0.20	0.19
V_{reac} [m^3]	20×10^{-3}	20×10^{-3}
L [m]	1.4	0.7
I'' [Einst $\cdot m^{-2} \cdot s^{-1}$]	3.6×10^{-4}	
I [Einst $\cdot s^{-1}$]	6.5×10^{-4}	6.5×10^{-4}
C_0 [mol $\cdot m^{-3}$]	2	2
ϕ_{vL} [$m^3 \cdot s^{-1}$]	$1 \times 10^{-5} - 1 \times 10^{-3}$	$1 \times 10^{-5} - 2 \times 10^{-3}$
v_L [$m \cdot s^{-1}$]	$7 \times 10^{-4} - 7 \times 10^{-2}$	$3.5 \times 10^{-4} - 7 \times 10^{-2}$
ϕ_{vG} [$m^3 \cdot s^{-1}$]	$1 \times 10^{-5} - 1 \times 10^{-3}$	$1 \times 10^{-5} - 2 \times 10^{-3}$
v_G [$m \cdot s^{-1}$]	$7 \times 10^{-4} - 7 \times 10^{-2}$	$3.5 \times 10^{-4} - 7 \times 10^{-2}$

The calculations are based on the light properties of Philips TL140W UV lamps (350–400 nm, $\lambda_{max} = 370$ nm, 37 W UV-A). The flow rates of the liquid and the gas phase are between 1×10^{-5} $m^3 \cdot s^{-1}$ and 2×10^{-3} $m^3 \cdot s^{-1}$, corresponding with a superficial velocity of 3.5×10^{-4} $m \cdot s^{-1}$ and 7×10^{-2} $m \cdot s^{-1}$ (see Table 2). The initial concentration of the pollutant is 2 $mol \cdot m^{-3}$.

Modeling of the Reactors

The conversion in the reactors is calculated from steady-state mass balances (Froment and Bischoff, 1979), combined with mass transfer and kinetic relations. The balance and mass-transfer equations (together with the boundary conditions) are presented in Table 3 for formic acid. Axial dispersion is not taken into account. The relations for the chemical kinetics are shown in Table 4.

In the kinetic relations the influence of the catalyst loading, the light intensity, and the oxygen concentration are taken into account next to the concentration of the pollutant (see Table 4). In photocatalysis the catalyst has to be illuminated before it becomes active; the light activates the catalyst by generating electron–hole pairs. Therefore, the light intensity and catalyst loading have to be included in the kinetic model to obtain a reactor-independent model that can be used for the design of a photocatalytic reactor. Oxygen plays an important role in photocatalytic degradation. It is necessary both for the reaction with the formic acid radical ($HCOO^{\bullet}$) and for capturing the electrons to prevent them from recombining with the holes. The hole can then form hydroxyl radicals which can attack almost any organic pollutant and degrade it totally to carbon dioxide, water, and mineral acids (Dijkstra et al., 2002).

In the PBR there is an important gradient of the light intensity in the radial direction. This is taken into account by considering that the reactor consists of seven concentric annular sections with radius R_c: the greater part of the conversion takes place in the illuminated innermost section. The liquid moves between the "illuminated" and "dark" compartments by radial dispersion. Such radial effects do not occur in the other reactors.

The kinetic parameters, k_{PBR}, $K_{PBR,FA}$, and K_{PBR,O_2}, were determined in an earlier study (Dijkstra et al., 2002; Dijkstra, 2002) and are presented in Table 5. The reaction rate is dependent on the LVREA, the local volumetric rate of energy absorption (Cassano et al., 1995), which is a measure for the amount of radiation absorbed by the catalyst (see Table 4). This value is determined with the two-flux model (Raupp et al., 1997; Dijkstra, 2002). For the radial dispersion coefficient, the relation for the Péclet group presented by Gunn (1987) is used and the gas–liquid mass-transfer coefficient, $k_{GL}a_B$ is described with the relation of Reiss (1967), see the Appendix. The relations for the liquid–solid mass-transfer coefficient, k_L, in a two-phase (L-S) and three-phase (G-L-S) packed-bed reactor are also presented in the Appendix.

A different kinetic relation is applied in the TR and MR (see Table 4). The values of the kinetic parameters, k_R, K_{FA},

Table 3. Overview of Models for PBR, FR, MR, and TR

PBR: Model

$$v_L \frac{dC_{b,\mathrm{FA}}}{dz} = \epsilon_{\mathrm{bed}} D_{\mathrm{rad,FA}} \left(\frac{\partial^2 C_{b,\mathrm{FA}}}{\partial r^2} + \frac{1}{r} \frac{\partial C_{b,\mathrm{FA}}}{\partial r} \right) - R$$

$$v_L \frac{dC_{b,\mathrm{O_2},L}}{dz} = \epsilon_{\mathrm{bed}} D_{\mathrm{rad,O_2}} \left(\frac{\partial^2 C_{b,\mathrm{O_2},L}}{\partial r^2} + \frac{1}{r} \frac{\partial C_{b,\mathrm{O_2},L}}{\partial r} \right) - 0.5R + k_{GL} a_B (m C_{\mathrm{O_2},G} - C_{b,\mathrm{O_2},L})$$

$$v_G \frac{dC_{\mathrm{O_2},G}}{dz} = - k_{GL} a_B (m C_{\mathrm{O_2},G} - C_{b,\mathrm{O_2}L})$$

PBR: Boundary conditions

$C_{b,A,L} = C_{b,A,L,0}$ at $z = 0$ and $R_i \le r \le R_c$

$\frac{\partial C_{b,A,L}}{\partial r} = 0$ at $r = R_i$ and $r = R_c$ for $0 \le z \le \mathrm{L}$

$C_{\mathrm{O_2},G} = C_{\mathrm{O_2},G,0}$ at $z = 0$

FR, MR, TR: Model

$$v_L \frac{dC_{b,FA}}{dz} = - R$$

$$v_L \frac{dC_{b,\mathrm{O_2},L}}{dz} = -0.5R + k_{GL} a_B (m C_{\mathrm{O_2},G} - C_{b,\mathrm{O_2},L})$$

$$v_G \frac{dC_{\mathrm{O_2},G}}{dz} = - k_{GL} a_B (m C_{\mathrm{O_2},G} - C_{b,\mathrm{O_2},L})$$

FR, MR, TR: Boundary conditions

$C_{b,\mathrm{FA}} = C_{b,\mathrm{FA},0}$ at $z = 0$

$C_{b,\mathrm{O_2},L} = C_{b,\mathrm{O_2},L,0}$ at $z = 0$

$C_{\mathrm{O_2},G} = C_{\mathrm{O_2},G,0}$ at $z = 0$

PBR, FR, MR, TR: Mass transfer

$k_{L,\mathrm{FA}} a (C_{b,\mathrm{FA}} - C_{s,\mathrm{FA}}) = R$

$k_{L,\mathrm{O_2}} a (C_{b,\mathrm{O_2},L} - C_{s,\mathrm{O_2},L}) = 0.5R$

and $K_{\mathrm{O_2}}$, were determined for the TR in a previous study (Dijkstra et al., 2002) (see Table 5). The value of $k_{GL}a_B$ in the TR is estimated with a relation for mass-transfer coefficients in a bubble column (see the Appendix). The values for the mass-transfer coefficient in a three-phase system are estimated with equations previously determined in a tubular reactor (Dijkstra et al., 2002) and for a two-phase system with the relation of Yapici and Ozbahar (1998), (see the Appendix).

Light absorption in a fiber is quantified by the refractive loss coefficient, α_f, which is a function of the optical and physical properties of the fiber core and the photocatalytic coating (m^{-1}). For an amount of catalyst of 2 $\mathrm{g \cdot m^{-2}}$ ($d_L = 1.3$ μm), the refractive loss index is estimated to be 10 m^{-1} (Peill and Hoffmann, 1995, 1998). Relations for the determination of $k_{GL}a_B$ and k_L in the FR are presented in the Appendix. No relation for k_L in a three-phase FR could be found. The relation for the two-phase system is, therefore, also used in the three-phase system.

In the membrane reactor no mass-transfer limitation will occur, since the mass transfer in the membrane will be determined by convection instead of diffusion due to the forced flow through the membrane. For the kinetic model it is assumed that the model of the TR can be used. The value of $k_{GL}a_B$ is again estimated with a relation for mass-transfer coefficients in a bubble column (see the Appendix). A part of the radiation energy is lost due to absorption by the water and an extra phase transfer from the liquid to the solid membrane. According to Braun et al. a phase transfer costs 4% of the energy (Braun et al., 1991). Therefore, the intensity in the membrane is 4% lower than in the TR, neglecting the radiation absorbed by the water.

Table 5. Values of Kinetic Parameters

PBR		TR and FR	
k_{PBR}	0.64	k_R	1.37
$K_{\mathrm{PBR,FA}}$ [$\mathrm{m^3 \cdot mol^{-1}}$]	3.35	K_{FA} [$\mathrm{m^5 \cdot g^{-1} \cdot mol^{-1}}$]	0.71
$K_{\mathrm{PBR,O_2}}$ [$\mathrm{m^3 \cdot mol^{-1}}$]	3.62	$K_{\mathrm{O_2}}$ [$\mathrm{m^3 \cdot mol^{-1}}$]	3.62

Source: Dijkstra et al. (2002) and Dijkstra (2002).

Results and Discussion

Reactor configuration

The performance of the PBR is optimized for the particle diameter and catalyst loading. The performance with large particles (2 mm) is slightly better than with small particles (1.3 mm). The conversion increases with catalyst loading and levels off for loadings above 1 $\mathrm{g \cdot m^{-2}}$. The results discussed below are obtained with a particle diameter of 2 mm and a catalyst loading of 2 $\mathrm{g \cdot m^{-2}}$, which gives the highest conversion.

Table 4. Kinetic Models in PBR, FR, MR and TR

Reactor	Kinetic Model	Reference
PBR	$R = k_{\mathrm{PBR}} e L V R E A(r) \frac{K_{\mathrm{PBR,FA}} C_{s,\mathrm{FA}}}{1 + K_{\mathrm{PBR,FA}} C_{s,\mathrm{FA}}} \frac{K_{\mathrm{PBR,O_2}} C_{s,\mathrm{O_2},L}}{1 + K_{\mathrm{PBR,O_2}} C_{s,\mathrm{O_2}L}}$	(Dijkstra, 2002)
FR	$R = k_R e I''_{f,\mathrm{abs}}(z) a_{\mathrm{ext}} \frac{w_{\mathrm{cat}} K_{\mathrm{FA}} C_{s,\mathrm{FA}}}{1 + w_{\mathrm{cat}} K_{\mathrm{FA}} C_{s,\mathrm{FA}}} \frac{K_{\mathrm{O_2}} C_{s,\mathrm{O_2},L}}{1 + K_{\mathrm{O_2}} C_{s,\mathrm{O_2},L}}$	
	$I''_{f,\mathrm{abs}}(z) = \alpha_f \frac{I_f}{\pi d_f} e^{-\alpha_f z}$	(Peill and Hoffmann, 1998)
MR, TR	$R = k_R e g a_{\mathrm{ext}} \frac{w_{\mathrm{cat}} K_{\mathrm{FA}} C_{s,\mathrm{FA}}}{1 + w_{\mathrm{cat}} K_{\mathrm{FA}} C_{s,\mathrm{FA}}} \frac{K_{\mathrm{O_2}} C_{s,\mathrm{O_2},L}}{1 + K_{\mathrm{O_2}} C_{s,\mathrm{O_2},L}}$	(Dijkstra et al., 2002)
	$g = \int_{\lambda_1}^{\lambda_2} (I''_\lambda - I''_\lambda e^{-\alpha_\lambda d_L})\, d\lambda$	

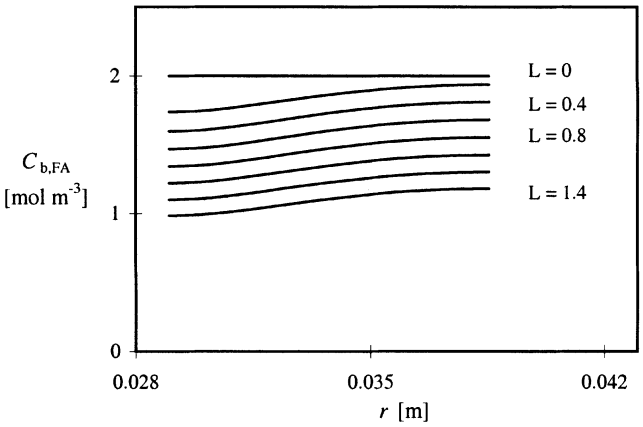

Figure 3. Radial concentration profiles of formic acid in the PBR for different axial positions in reactor.

$v_G = v_L = 7\times10^{-3}$ m·s^{-1}, air addition.

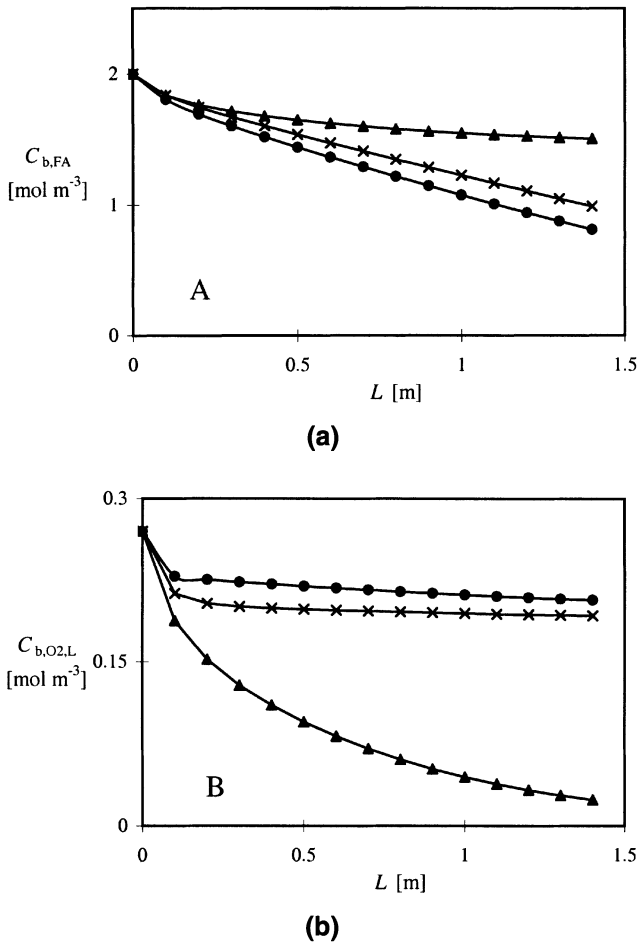

Figure 4. Concentration profiles in the PBR as a function of v_G ($v_L = 7\times10^{-3}$ m·s^{-1}, air addition).

▲: $v_G = 0$ m·s^{-1}; ×: $v_G = 0.007$ m·s^{-1}; ●: $v_G = 0.07$ m·s^{-1}. (A) Formic acid concentration vs. length; (B) oxygen concentration in the liquid phase vs. length.

Radial dispersion hardly influences the performance of the reactor. If this effect is neglected, the conversion is equal to 48.5% instead of 45% for v_G, and v_L is 7×10^{-3} m·s^{-1} with the addition of air. Figure 3 shows the radial concentration profiles for different axial positions in the reactor.

Increasing the layer thickness in the TR increases the reaction rate over the whole range studied. As we can see in Table 4, the generation rate of charge carriers (g) increases with increasing layer thickness (d_L), until all the light is absorbed for thick layers. For the range of catalyst loading studied (maximum 2 g·m^{-2}, corresponding to $d_L = 1.3$ μm), this maximum light absorption is not yet obtained. In a previous study it was found that the reaction rate in the range of layer thicknesses studied ($d_L < 2$ μm) increased with increasing catalyst loading due to an increase in adsorption sites [$\theta_{FA} = w_{cat} K_{FA} C_{s,FA} / (1 + w_{cat} K_{FA} C_{s,FA})$] (Dijkstra et al., 2002). The performance of the reactor is further studied for a loading of 2 g·m^{-2}.

Increasing the number of fibers in the FR increases the conversion. Due to a lower light flux, mass-transfer limitation will be less, and thus the conversion increases (see below). Increasing the catalyst loading on the fiber will result in a higher α_f (Peill and Hoffmann, 1995, 1998). The conversion is reduced slightly by increasing α_f from 10 to 20. The optimal amount of the catalyst has not been determined, due to a lack of information about α_f for lower amounts of catalyst.

Influence of oxygen

The addition of extra oxygen has a large influence on the performance of the reactors. Figure 4 shows the concentration profiles of formic acid and oxygen along the reactor length in the PBR for different v_G (air addition). In the absence of a third phase, the oxygen concentration decreases rapidly and the decrease in formic acid levels off. When air is added, the oxygen concentration remains high enough for the reaction to proceed. The degradation rate of formic acid is higher for the highest air flow, since then $C_{b,O_2,L}$ is also higher.

Figure 5 shows the conversion of formic acid in the PBR for the addition of pure oxygen, air, and no extra gas addi-

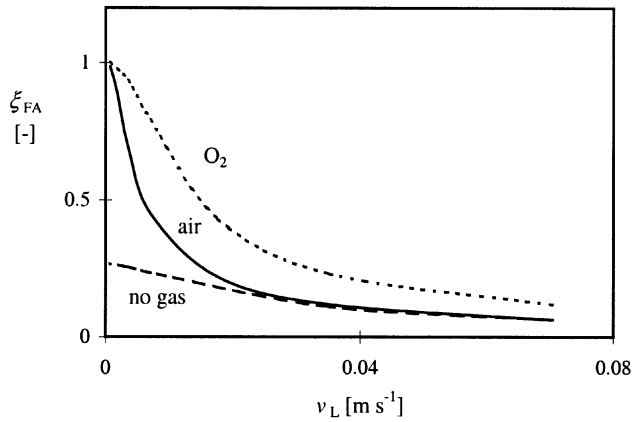

Figure 5. Conversion of formic acid in the PBR as a function of v_L.

— air; ---- oxygen; ——— no gas. ($v_G = 0.007$ m·s^{-1}.)

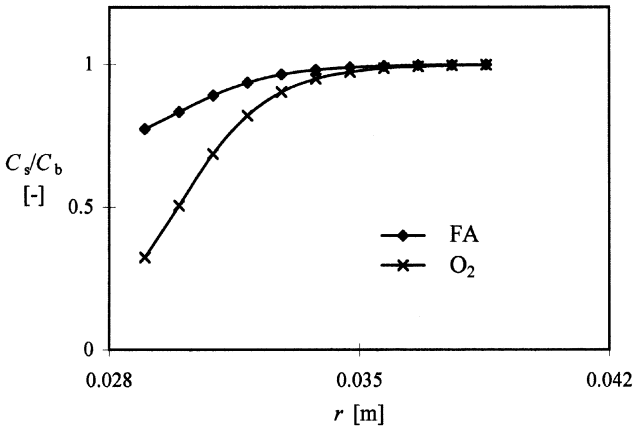

Figure 6. C_s/C_b ratio of oxygen and formic acid in radial direction in the PBR at $L = 0.1$

$v_G = v_L = 7 \times 10^{-3}$ m·s^{-1}, air addition.

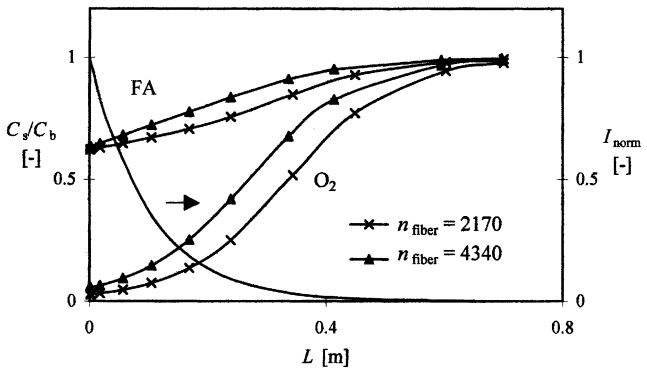

Figure 7. C_s/C_b ratio of oxygen and formic acid and the normalized light intensity as a function of axial coordinate in the FR.

$v_G = v_L = 0.007$ m·s^{-1}, air addition.

tion. It is clear that much higher conversions can be obtained when a gas phase is added for the degradation of formic acid. The addition of pure oxygen results in the highest conversion. A previous study showed that for a three-phase packed-bed reactor on a pilot or industrial scale, a coating method has to be developed with improved adherence and similar catalyst activity (Dijkstra et al., 2001).

Mass-transfer limitation

The degree of liquid–solid mass-transfer limitation of a certain compound can be determined with the ratio of the surface to bulk concentration of that compound. This ratio is equal to 1 for no mass-transfer limitation and to 0 for complete mass-transfer limitation. In the PBR, this effect can occur in the vicinity of the wall where the radiation is maximal. The $C_{s,O_2}/C_{b,O_2}$ and $C_{s,FA}/C_{b,FA}$ ratios are given as a function of the radius in Figure 6. In the vicinity of the wall the C_s/C_b ratio of both components is smaller than 1, which indicates some mass-transfer limitation. Oxygen is more mass-transfer limited than formic acid, because the oxygen concentration in the bulk is lower.

In the TR the $C_{s,O_2}/C_{b,O_2}$ is 0.04 and $C_{s,FA}/C_{b,FA}$ ratio is about 0.6 along the reactor length: the reaction is mass-transfer limited in oxygen (for v_L and v_G 0.007 m·s^{-1} with the addition of air). Increasing v_L and v_G to 0.07 m·s^{-1} increases the oxygen ratio to 0.26 and the formic acid ratio to 0.7 due to higher mass transfer. If pure oxygen is added, the degree of the mass-transfer limitation of oxygen decreases further ($C_{s,O_2}/C_{b,O_2} = 0.64$, v_L and v_G 0.007 m·s^{-1}). That of formic acid increases ($C_{s,FA}/C_{b,FA} = 0.27$), because now the formic acid concentration is lower than the oxygen concentration. Baffles that increase the turbulence can be placed in the reactor to reduce the mass-transfer limitation.

Also in the fiber reactor the C_s/C_b ratios show a high degree of mass-transfer limitation for the degradation of formic acid (see Figure 7). Since the radiation decreases along the fiber, the activity will also decrease along the fiber. Therefore, the C_s/C_b ratios will increase along the reactor length. Increasing the number of fibers decreases the radiation flux in the fibers, and thus the reaction rate; the extent of the mass-transfer limitation decreases also (see Figure 7).

Calculations in previous work showed that the internal diffusion limitation can occur for thick layers and high light intensities (Dijkstra et al., 2002). The extent of the internal mass-transfer limitation can be estimated with the effectiveness factor, η, with no and with complete diffusion limitation for $\eta = 1$ and 0, respectively. For the kinetic models in Table 4, the effectiveness factor can be estimated for two limiting situations (Dijkstra et al., 2002): the oxygen concentration is much lower than the formic acid concentration, which makes oxygen the limiting component, and vice versa. The effectiveness factor in the TR has been determined for these two limiting situations. It has a value between 0.8 and 1 for most of the modeling ($w_{cat} = 2$ g·m^{-2}). If the oxygen concentration approaches zero, the effectiveness factor will decrease to a minimum value of 0.65. This again emphasizes the necessity of keeping the oxygen concentration as high as possible in the reactor.

In the fiber reactor the radiation flux in the beginning of the reactor is a factor of 3 higher than in the TR. Therefore, internal diffusion limitation probably occurs in the first part of the fiber. If the number of fibers in the reactor is increased, this effect will be less due to the decreased radiation flux per fiber. The same amount of radiation is absorbed in the PBR, whereas the catalyst area is much larger than in the TR. Therefore the surface-related kinetic rate constant in the PBR is much lower than that in the TR and the internal mass-transfer limitation will be negligible (Dijkstra et al., 2001). In the MR, it is hard to estimate the extent of the internal diffusion limitation, because the configuration of the membrane is not very well known.

Performance of reactors

Figure 8 gives the conversions of formic acid as a function of the superficial liquid velocity in the four reactors. The conversion depends strongly on the flow rate of the liquid through the reactor; for a high conversion, the flow rate should not be too high. The membrane reactor clearly has the highest conversion, due to the absence of mass-transfer limitation in this reactor. Regarding this result, however, it has to be borne in mind that the degradation in this reactor is not experimentally verified. Both the FR and TR show a poor performance

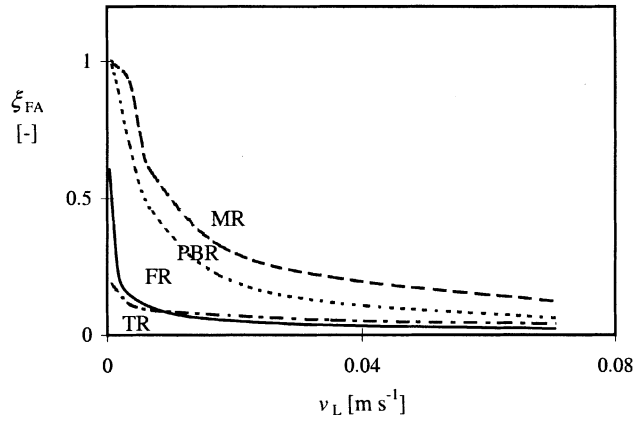

Figure 8. Conversion of formic acid in the four reactors as a function of v_L.

$v_G = 7 \times 10^{-3}$ m·s^{-1}, air addition. ——— MR; ---- PBR; — FR; -·-· TR.

when compared to the MR and PBR, due to the severe external mass-transfer limitation in the FR and TR.

The increase of v_G has a large influence in the MR and PBR (see Figure 9). Increasing v_G in these two reactors will increase $C_{b,O_2,L}$, and thus the conversion. Due to the low conversion in the TR and FR, the oxygen concentration in the liquid phase will remain almost constant, also for low v_G. Therefore, the increase of v_G has hardly any influence. The conversion increases with v_G in the TR only because of an increased mass-transfer coefficient.

The efficiency of the energy consumption (UV-A energy entering the reactor divided by the total lamp energy use) in the fiber reactor of Peill and Hoffmann is 0.0001, meaning that 0.01% of the energy used by the 1,000-W Xe arc lamp is actually used in the reactor. This value is extremely low compared to the PBR, MR, and TR, which use approximately 23% of the energy of the 140-W Philips TL140W/10 lamp. It may be possible to further optimize the fiber reactor with respect to light efficiency. Both the MR and PBR will have a larger pressure drop over the reactor than the FR and TR will, which will increase the costs of the necessary pumps.

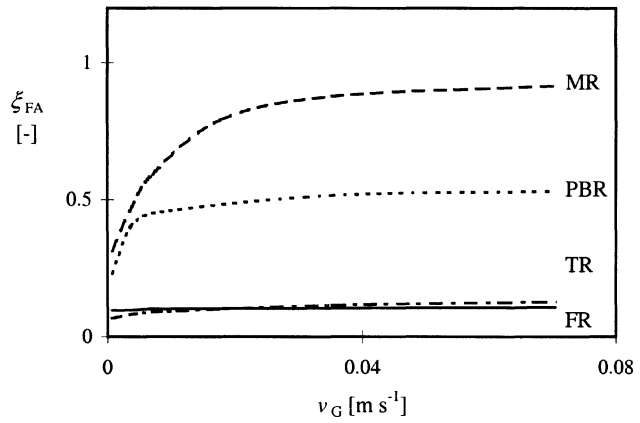

Figure 9. Conversion of formic acid in the four reactors as a function of v_G.

$v_L = 7 \times 10^{-3}$ m·s^{-1}, air addition. ——— MR; ---- PBR; — FR; -·-· TR.

Axial dispersion

Axial dispersion has been neglected in the modeling. According to Froment and Bischoff (1979), this assumption can be made for packed-bed reactors if $L/d_p > 50$ (as in the PBR). Axial dispersion can play a role in bubble-column reactors. In the TR and MR, axial dispersion will negatively affect the conversion. To prevent this effect, baffles can be placed in the reactor. Modeling showed that five baffles are sufficient to maintain plug-flow behavior in the TR. In the fiber reactor, axial mixing will positively affect the conversion. Back mixing causes the fluid to reach the part of the fiber reactor with a higher intensity, which will cause a higher conversion. This effect is not quantified.

Conclusions

The performance of four different photocatalytic reactors (packed-bed, fiber, membrane, and tubular) was modeled assuming that the process is taking place on a pilot scale for the degradation of formic acid in deionized water. The influence of radial dispersion (PBR), external mass transfer, flow rate, catalyst loading, and the oxygen concentration are taken into account. The addition of air increases the conversion of formic acid by maintaining oxygen in the liquid. When pure oxygen was added instead of air, the conversion again increased considerably, due to the higher oxygen concentration. The MR and PBR show a better performance than the FR and TR. Mass-transfer limitation severely decreases the conversion in the TR and FR. The PBR suffers little mass-transfer limitation, and this effect does not occur in the MR. The performance of the PBR was barely influenced by the radial dispersion caused by the radial light intensity profile. More research has to be done for the MR to confirm the results. The PBR, MR, and TR show a much better energy efficiency than the FR.

Acknowledgments

This work was supported by the Netherlands Foundation for Chemical Research (SON) with financial aid from the Netherlands Technology Foundation. We acknowledge the generous supply of UV lamps by Philips, Eindhoven.

Notation

a_B = gas–liquid interfacial area per unit reactor volume, $m^2 \cdot m_{reac}^{-3}$
a_{ext} = specific external surface area in TR, MR, and FR, $m_{cat}^2 \cdot m_{reac}^{-3}$
a = specific external surface area, $m_{cat}^2 \cdot m_{reac}^{-3}$
Bo = Bond number defined by Eq. A5d
C = concentration, mol·m^{-3}
C = coefficient in Eq. A5a
C_s = surface concentration, mol·m^{-3}
C_b = bulk concentration, mol·m^{-3}
d_f = diameter fiber, m
d_h = hydraulic diameter, m
d_i = diameter inner tube, m
d_L = layer thickness, m
d_{LL} = distance between lamps, m
d_p = particle diameter, m
d_{pe} = equivalent particle diameter, m
d_r = diameter reactor, m

D_A = diffusivity of component A, $m^2 \cdot s^{-1}$
D_{rad} = radial dispersion coefficient, $m^2 \cdot s^{-1}$
e = equivalence constant (equal to 1), $mol \cdot Einst^{-1}$
f_{LG} = two-phase friction factor
Fr = Froude number ($= v_G^2/d_h g$)
g = generation rate of charge carriers, $Einst \cdot m^{-2} \cdot s^{-1}$
g = gravitational acceleration, $m \cdot s^{-2}$
I = total number of photons entering reactor, $Einst \cdot s^{-1}$
I_λ = total number of photons entering reactor per wavelength, $Einst \cdot s^{-1} \cdot nm^{-1}$
I'' = light flux entering reactor, $Einst \cdot m^{-2} \cdot s^{-1}$
I_f = light intensity entering fibers, $Einst \cdot s^{-1}$
$I''_{f,ads}$ = absorbed radiation in fiber, $Einst \cdot m^{-2} \cdot s^{-1}$
I_{norm} = normalized light intensity
I''_λ = light flux entering reactor per wavelength, $Einst \cdot m^{-2} \cdot s^{-1} \cdot nm^{-1}$
k_L = mass-transfer coefficient for liquid-to-solid phase, $m \cdot s^{-1}$
k_{GL} = mass-transfer coefficient for gas-to-liquid phase, $m \cdot s^{-1}$
k_{PBR} = kinetic constant in PBR
k_R = kinetic constant in FR, MR, and TR
$K_{PBR,A}$ = kinetic constant in PBR, component A (see Table 5)
K_A = kinetic constant in FR, MR, and TR, component A (see Table 5)
L = reactor length, m
$LVREA$ = local volumetric rate of energy absorption, $Einst \cdot m^{-3} \cdot s^{-1}$
m = distribution coefficient of oxygen, such as $C_L = mC_g$
n_{fiber} = number of fibers
Pe_A = Péclet number ($= v_L d_p/\epsilon_{bed} D_A$)
Pe_f = defined by Eq. A10
r = radial coordinate, m
R = reaction rate per unit reactor volume, $mol \cdot m^{-3}_{react} \cdot s^{-1}$
R_c = radius of concentric cylinder around tube, m
R_i = radius of glass tube surrounding lamp, m
Re = Reynolds number in Eq. A5b ($= \rho_L v_G d_h/\eta_L$)
Re_f = Reynolds number in FR ($= \rho v_f d_f/\eta$)
Re_G = Reynolds number gas ($= \rho_G v_G d_h/\eta_G$)
Re_L = Reynolds number liquid ($= \rho_L v_L d_h/\eta_L$)
Re_p = Reynolds number in PBR ($= \rho v d_p/\eta$)
Sc_A = Schmidt number ($= \eta_L/D_A \rho_L$)
Sh_A = Sherwood number ($= k_L d_h/D_A$)
Sh_{BA} = Sherwood number in bubble column ($= k_L a_B d_h^2/D_A$)
Sh_{fA} = Sherwood number in FR ($= k_L d_f/D_A$)
Sh_{pA} = Sherwood number in PBR ($= k_L d_p/D_A$)
v = superficial velocity (PBR, FR, and MR, empty column), $m \cdot s^{-1}$
v_f = velocity past fibers, $m \cdot s^{-1}$
V_{reac} = reactor volume, m^3
w_{cat} = catalyst loading, $g \cdot m^{-2}$
z = axial coordinate in reactor, m
Z = coefficient in Eq. A13

Greek letters

α_f = refractive loss coefficient of fiber, m^{-1}
α_λ = optical absorption coefficient of catalyst, m^{-1}
δ_{LG} = frictional pressure gradient per unit height of column, $dyne \cdot cm^{-3}$
ϵ_{bed} = porosity of packed-bed reactor
ϵ_G = gas holdup
η = effectiveness factor
η = viscosity, $Pa \cdot s$
θ_{FA} = adsorption term of formic acid
λ = wavelength of light, nm
λ_{max} = wavelength of light with maximum light intensity, nm
ξ_{FA} = conversion of formic acid at reactor outlet, %
ρ = density, $kg \cdot m^{-3}$
σ = interfacial tension, $N \cdot m^{-1}$
τ = tortuosity
ϕ_v = flow rate, $m^3 \cdot s^{-1}$

Subscripts and superscripts

A = component A
FA = formic acid
FR = fiber reactor
G = gas
L = liquid
MR = membrane reactor
O_2 = oxygen
PBR = packed bed reactor
TR = tubular reactor
WW = wastewater
0 = initial conditions

Literature Cited

Al-Ekabi, H., and N. Serpone, "Kinetic Studies in Heterogeneous Photocatalysis: 1. Photocatalytic Degradation of Chlorinated Phenols in Aerated Aqueous Solutions over TiO_2 Supported on a Glass Matrix," *J. Phys. Chem.*, **92**, 5726 (1988).

Bahnemann, D., "Photocatalytic Detoxification of Polluted Waters," *The Handbook of Environmental Chemistry*, P. Boule, ed., Vol. 2, Part L, Springer, Berlin, p. 285 (1999).

Bellobono, I. R., B. Barni, and F. Gianturco, "Pre-Industrial Experience in Advanced Oxidation and Integral Photodegradation of Organics in Potable Waters and Waste Waters by PHOTOPERM™ Membranes Immobilizing Titanium Dioxide and Promoting Photocatalysts," *J. Memb. Sci.*, **102**, 139 (1995).

Bellobono, I. R., F. Gianturco, C. M. Chiodaroli, M. L. Raimondi, A. Moroni, and B. Gawlik, "Pilot-Plant Photomineralization of Atrazine in Aqueous Solution, by Photocatalytic Membranes Immobilizing Titanium Dioxide and Promoting Photocatalysts," *Fresenius' Environ. Bull.*, **6**, 461 (1997).

Bellobono, I. R., P. L. Pinacci, G. Riva, and C. Lagrasta, "Pilot-Plant Photomineralization of s-Triazines in Aqueous Solution, by Photocatalytic Membranes Immobilising Titanium Dioxide and Trialkyl Vanadates Photocatalysts," *Fresenius' Environ. Bull.*, **7**, 277 (1998).

Boyes, A. P., S. Raymahasay, A. T. Sulidis, and J. M. Winterbottom, "Oxidation of Aqueous Organic Pollutants in Industrials Waste Water by Heterogeneous Photocatalysis Using a Cocurrent Downflow Bubble Column Contactor (CDC)," *Int. Conf. on Water Pollution III: Modelling, Measuring and Prediction*, Computational Mechanics Publications, Southampton, p. 313 (1997).

Braun, A. M., M.-T. Maurette, and E. Oliveros, *Photochemical Technology*, Wiley, Chichester (1991).

Cassano, A. E., C. A. Martin, R. J. Brandi, and O. M. Alfano, "Photoreactor Analysis and Design: Fundamentals and Applications," *Ind. Eng. Chem. Res.*, **34**, 2155 (1995).

Cussler, E. L., *Diffusion, Mass Transfer in Fluid Systems*, 2nd ed., Cambridge Univ. Press, Cambridge, p. 427 (1997).

Dibble, L. A., and G. B. Raupp, "Fluidized-Bed Photocatalytic Oxidation of Trichloroethylene in Contaminated Airstreams," *Environ. Sci. Technol.*, **26**, 492 (1992).

Dijkstra, M. F. J., "Development of a Continuous Photocatalytic Reactor," PhD Thesis, Univ. of Groningen, Groningen, The Netherlands (2002).

Dijkstra, M. F. J., H. Buwalda, A. W. F. de Jong, A. Michorius, J. G. M. Winkelman, and A. A. C. M. Beenackers, "Experimental Comparison of Three Reactor Designs for Photocatalytic Water Purification," *Chem. Eng. Sci.*, **56**, 547 (2001).

Dijkstra, M. F. J., H. J. Panneman, J. G. M. Winkelman, J. J. Kelly, and A. A. C. M. Beenackers, "Modeling the Photocatalytic Degradation of Formic Acid in a Reactor with Immobilized Catalyst," *Chem. Eng. Sci.*, **57**, 4895 (2002).

Dionysiou, D. D., A. P. Khodadoust, A. M. Kern, M. T. Suidan, I. Baudin, and J. M. Laîné, "Continuous-Mode Photocatalytic Degradation of Chlorinated Phenols and Pesticides in Water Using a Bench-Scale TiO_2 Rotating Disk Reactor," *Appl. Catal. B*, **24**, 139 (2000).

Dudley, J., "Mass Transfer in Bubble Columns: A Comparison of Correlations," *Water Res.*, **29**, 1129 (1995).

Fabiyi, M. E., and R. J. Skelton, "The Application of Oscillatory Flow Mixing to Photocatalytic Wet Oxidation," *J. Photochem. Photobiol. A*, **129**, 17 (1999).

Froment, G. F., and K. B. Bischoff, *Chemical Reactor Analysis and Design*, Wiley, New York (1979).

Gianturco, F., and L. Vianelli, "Pilot-Plant Photomineralization of Dichloromethane and Tetrachloroethene in Aqueous Solution, by

Photocatalytic Membranes Immobilizing Titanium Dioxide and Photopromoters," *Chemosphere*, **33**, 1531 (1996).
Gunn, D. J., "Axial and Radial Dispersion in Fixed Beds," *Chem. Eng. Sci.*, **42**, 363 (1987).
Haarstrick, A., O. M. Kut, and E. Heinzle, "TiO_2-Assisted Degradation of Environmentally Relevant Organic Compounds in Wastewater Using a Novel Fluidized Bed Photoreactor," *Environ. Sci. Technol.*, **30**, 817 (1996).
Halmann, M. M., *Photodegradation of Water Pollutants*, CRC Press, Boca Raton, FL (1996).
Herrmann, U., and G. Emig, "Liquid Phase Hydrogenation of Maleic Anhydride to 1,4-Butanediol in a Packed Bed Bubble Column Reactor," *Ind. Eng. Chem. Res.*, **37**, 759 (1998).
Hoffmann, M. R., S. T. Martin, W. Choi, and D. W. Bahnemann, "Environmental Applications of Semiconductor Photocatalysis," *Chem. Rev.*, **95**, 69 (1995).
Hofstadler, K., R. Bauer, S. Novalic, and G. Heisler, "New Reactor Design for Photocatalytic Wastewater Treatment with TiO_2 Immobilized on Fused-Silica Glass Fibers: Photomineralization of 4-Chlorophenol," *Environ. Sci. Technol.*, **28**, 670 (1994).
Hossain, Md. M., G. B. Raupp, S. O. Hay, and T. N. Obee, "Three-Dimensional Developing Flow Model for Photocatalytic Monolith Reactors," *AIChE J.*, **45**, 1309 (1999).
Karpel Vel Leitner, N., E. Le Bras, E. Foucault, and J.-H. Bousgarbìes, "A New Photochemical Reactor Design for the Treatment of Absorbing Solutions," *Proc. Int Conf. on Oxidation Technology for Water and Wastewater Treatment*, A. Vogelpohl, ed., Clausthal-Zellerfeld Papierflieger, Clausthal (1996).
Kawase, Y., B. Halard, and M. Moo-Young, "Theoretical Prediction of Volumetric Mass Transfer Coefficients in Bubble Columns for Newtonian and Non-Newtonian Fluids," *Chem. Eng. Sci.*, **42**, 1609 (1987).
Lea, J., and A. A. Adesina, "Continuous Flow Bubble Column Reactor for the Photocatalytic Causticisation of Sodium Oxalate," *Chem. Eng. Sci.*, **54**, 2209 (1999).
Legrini, O., E. Oliveros, and A. M. Braun, "Photochemical Processes for Water Treatment," *Chem. Rev.*, **93**, 671 (1993).
Marigangeli, R. E., and D. F. Ollis, "Photo-Assisted Heterogeneous Catalysis with Optical Fibers {II}. Nonisothermal Single Fiber and Fiber Bundle," *AIChE J.*, **26**, 1000 (1980).
Matthews, R. W., "Kinetics of Photocatalytic Oxidation of Organic Solutes Over Titanium Dioxide," *J. Catal.*, **111**, 264 (1988).
Matthews, R. W., "Photocatalysis in Water Purification: Possibilities, Problems and Prospects," *Photocatalytic Purification and Treatment of Water and Air*, D. F. Ollis, and H. Al-Ekabi, eds., Elsevier, Amsterdam, p. 121 (1993).
Maurino, V., C. Minero, E. Pelizzetti, and M. Vincenti, "Using Sunlight to Fight Pollution," *Chimica Ind.*, **81**, 61 (1999).
Mazzarino, I., and P. Piccinini, "Photocatalytic Oxidation of Organic Acids in Aqueous Media by a Supported Catalyst," *Chem. Eng. Sci.*, **54**, 3107 (1999).
Mazzarino, I., P. Piccinini, and L. Spinelli, "Degradation of Organic Pollutants in Water by Photochemical Reactors," *Catal. Today*, **48**, 315 (1999).
Mills, A., and S. Le Hunte, "An Overview of Semiconductor Photocatalysis," *J. Photochem. Photobiol. A*, **108**, 1 (1997).
Ollis, D. F., and C. Turchi, "Heterogeneous Photocatalysis for Water Purification: Contaminant Mineralization Kinetics and Elementary Reactor Analysis," *Environ. Prog.*, **9**, 229 (1990).
Ollis, D. F., E. Pelizzetti, and N. Serpone, "Photocatalyzed Destruction of Water Contaminants," *Environ. Sci. Technol.*, **25**, 1522 (1991).
Peill, N. J., and M. R. Hoffmann, "Development and Optimization of a TiO_2-Coated Fiber-Optic Cable Reactor: Photocatalytic Degradation of 4-Chlorophenol," *Environ. Sci. Technol.*, **29**, 2974 (1995).
Peill, N. J., and M. R. Hoffmann, "Chemical and Physical Characterization of a TiO_2-Coated Fiber Optic Cable Reactor," *Environ. Sci. Technol.*, **30**, 2806 (1996).
Peill, N. J., and M. R. Hoffmann, "Mathematical Model of a Photocatalytic Fiber-Optic Cable Reactor for Heterogeneous Photocatalysis," *Environ. Sci. Technol.*, **32**, 398 (1998).
Perry, R. H., D. W. Green, and J. O'Hara Maloney, *Perry's Chemical Engineers' Handbook*, 7th ed., McGraw-Hill, New York (1997).
Pozzo, R. L., M. A. Baltanás, and A. E. Cassano, "Towards a Precise Assessment of the Performance of Supported Photocatalysts for Water Detoxification Processes," *Catal. Today*, **54**, 143 (1999).
Puma, G. L., and P. L. Yue, "A Laminar Falling Film Slurry Photocatalytic Reactor: I. Model Development," *Chem. Eng. Sci.*, **53**, 2993 (1998a).
Puma, G. L., and P. L. Yue, "A Laminar Falling Film Slurry Photocatalytic Reactor: II. Experimental Validation of the Model," *Chem. Eng. Sci.*, **53**, 3007 (1998b).
Puma, G. L., and P. L. Yue, "Enhanced Photocatalysis in a Pilot Laminar Falling Film Slurry Reactor," *Ind. Eng. Chem. Res.*, **38**, 3246 (1999).
Puma, G. L., and P. L. Yue, "The Modeling of a Fountain Photocatalytic Reactor with a Parabolic Profile," *Chem. Eng. Sci.*, **56**, 721 (2000).
Rajeshwar, K., "Photoelectrochemistry and the Environment," *J. Appl. Electrochem.*, **25**, 1067 (1995).
Ramachandran, P. A., and R. V. Chaudari, *Three-Phase Catalytic Reactors*, Gordon and Breach, London, p. 256 (1983).
Raupp, G. B., J. A. Nico, S. Annangi, R. Changrani, and R. Annapragada, "Two-Flux Radiation-Field Model for an Annular Packed-Bed Photocatalytic Oxidation Reactor," *AIChE J.*, **43**, 792 (1997).
Ray, A. K., "Design, Modelling and Experimentation of a New Large-Scale Photocatalytic Reactor for Water Treatment," *Chem. Eng. Sci.*, **54**, 3113 (1999).
Ray, A. K., and A. A. C. M. Beenackers, "Novel Photocatalytic Reactor for Water Purification," *AIChE J.*, **44**, 477 (1998a).
Ray, A. K., and A. A. C. M. Beenackers, "Development of a New Photocatalytic Reactor for Water Purification," *Catal. Today*, **40**, 73 (1998b).
Reiss, L. P., "Cocurrent Gas-Liquid Contacting in Packed Columns," *Ind. Eng. Chem. Proc. Des. Dev.*, **6**, 486 (1967).
Sauer, M. L., and D. F. Ollis, "Acetone Oxidation in a Photocatalytic Monolith Reactor," *J. Catal.*, **149**, 81 (1994).
Schiavello, M., *Heterogeneous Photocatalysis*, Vol. 3, Wiley Series on Photoscience and Photoengineering, Wiley, Chichester (1997).
Sclafani, A., A. Brucato, and L. Rizzuti, "Mass Transfer Limitations in a Packed Bed Photoreactor Used for Phenol Removal," *Photocatalytic Purification and Treatment of Water and Air*, D. F. Ollis and H. Al-Ekabi, eds., Elsevier, Amsterdam, p. 533 (1993).
Sczechowski, J. G., C. A. Koval, and R. D. Noble, "A Taylor Vortex Reactor for Heterogeneous Photocatalysis," *Chem. Eng. Sci.*, **50**, 3163 (1995).
Serpone, N., and E. Pellizetti, *Photocatalysis Fundamentals and Applications*, Wiley, New York (1989).
Serrano, B., and H. de Lasa, "Photocatalytic Degradation of Water Organic Pollutants. Kinetic Modeling and Energy Efficiency," *Ind. Eng. Chem. Res.*, **36**, 4705 (1997).
Serrano, B., and H. de Lasa, "Photocatalytic Degradation of Water Organic Pollutants: Pollutant Reactivity and Kinetic Modeling," *Chem. Eng. Sci.*, **54**, 3063 (1999).
Sobczyński, A., J. Gimenez, and S. Cervera-March, "Photodecomposition of Phenol in a Flow Reactor: Adsorption and Kinetics," *Monatsh. Chem.*, **128**, 1109 (1997).
Starosud, A., A. Bhargava, C. H. Langford, and A. Kantzas, "Development of New Photocatalytic Methods and Reactors for Waste Water Treatment," *Reaction Kinetics and the Development of Catalytic Processes*, G. F. Froment and K. C. Waugh, eds., Elsevier, Amsterdam (1999).
Topudurti, K., M. Wojciechowski, S. Anagnostopoulos, and R. Eilers, "Field Evaluation of a Photocatalytic Oxidation Technology," *Water Sci. Technol.*, **38**, 117 (1998).
Turpin, J. L., and R. L. Huntington, "Prediction of Pressure Drop for Two-Phase, Two-Component Concurrent Flow in Packed Beds," *AIChE J.*, **13**, 1196 (1967).
Winterbottom, J. M., Z. Khan, A. P. Boyes, and S. Raymahasay, "Photocatalyzed Oxidation of Phenol in Water Using a Cocurrent Downflow Contactor Reactor (CDCR)," *Environ. Prog.*, **16**, 125 (1997).
Winterbottom, J. M., Z. Khan, A. P. Boyes, and S. Raymahasay, "Catalytic Hydrogenation in a Packed Bed Bubble Column Reactor," *Catal. Today*, **48**, 221 (1999).
Yamazali-Nishida, S., K. J. Nagano, L. A. Philips, S. Cervera-March,

and M. A. Anderson, "Photocatalytic Degradation of Trichloroethylene in the Gas Phase Using Titanium Dioxide Particles," *J. Photochem. Photobiol. A*, **70**, 95 (1993).
Yapici, S., and R. E. Ozbahar, "Mass Transfer to Finite Areas at the Wall in Swirling Pipe Flow in the Transition Region," *Ind. Eng. Chem. Res.*, **37**, 643 (1998).
Yue, P. L., "Oxidation Reactors for Water and Wastewater Treatment," *Water Sci. Technol.*, **35**, 189 (1997).
Zhang, Y., J. C. Crittenden, D. W. Hand, and D. L. Perram, "Fixed-Bed Photocatalysts for Solar Decontamination of Water," *Environ. Sci. Technol.*, **28**, 435 (1994).

Appendix: Determination of Parameters for the Various Reactors

Membrane and tubular reactor

In the two-phase system, the solid–liquid mass-transfer coefficient, k_L, is estimated with a relation for the Sherwood number developed by Yapici and Ozbahar for a decaying swirling flow (Yapici and Ozbahar, 1998):

$$Sh_A = 0.095 Re_L^{0.75} Sc_A^{0.33} \tag{A1}$$

in which the definition of Sh_A is $k_L d_h/D_A$ and the definition of Sc_A is $\eta_L/\rho_L D_A$.

The solid–liquid mass-transfer coefficients for formic acid and oxygen in the three-phase system are calculated with relations experimentally determined in a tubular reactor (Dijkstra et al., 2002)

$$k_{L,FA} = 2.22\times10^{-7} Re_L^{0.73} Re_G^{0.124} \tag{A2}$$

$$k_{L,O_2} = 3.19\times10^{-7} Re_L^{0.73} Re_G^{0.124} \tag{A3}$$

where Re_L is $\rho_L v_L d_h/\eta_L$, and Re_G is $\rho_G v_G d_h/\eta_G$.

Dudley (1995) recommended the relation of Kawase et al. (1987) for determining the gas–liquid mass transfer in a bubble column. This relation is used for the three-phase TR and MR

$$Sh_{BA} = \frac{k_{GL} a_B d_h^2}{D_A} = \frac{12C}{\sqrt{\pi}} \sqrt{1.07}\, Sc_A^{1/2} Re^{3/4} Fr^{7/60} Bo^{3/5} \tag{A4}$$

with

$$C = 0.0645 n^{3/2}, \qquad Re = \frac{d_h v_G \rho_L}{\eta_L}, \qquad Fr = \frac{v_G^2}{d_h g},$$

$$Bo = \frac{g d_h^2 \rho_L}{\sigma} \tag{A5a–5d}$$

with $n = 1$ for water. For the determination of $k_{GL}a_B$ in the MR, the superficial velocity is based on the area of the annular space minus the area of the membranes, instead of being based on the empty column, as is done in the rest of the modeling.

Packed-bed reactor

The following relation of the Sh_{pA} number is used to determine the value of the mass-transfer coefficient, k_L, in the two-phase system (Perry, 1997)

$$Sh_{pA} = \frac{0.455}{\epsilon_{\text{bed}}} Re_{pL}^{0.598} Sc_A^{1/3} \tag{A6}$$

Here Sh_{pA} is $k_L d_p/D_A$, Re_{pL} is $\rho v_L d_p/\eta_L$, and ϵ_{bed} is the porosity of the packed bed. This relation is valid for liquids and gases with $10 < Re_{pL} < 2{,}000$. The relation of Colquhoun-Lee and Stepanek (Ramachandran and Chaudari, 1983) is used to calculate k_L in the three-phase system

$$\frac{k_L d_p}{D_A} = 0.155 Sc^{1/3} \left[\frac{\nu_L \delta_{LG} d_p^4 \rho_L^2}{\eta_L^3 \left(\frac{\epsilon_G}{\epsilon_{\text{bed}}} \left[\frac{\rho_G}{\rho_L} \left(\frac{v_G}{v_L} \right)^3 - 1 \right] + 1 \right)} \right]^{0.28} \tag{A7}$$

Here ϵ_G is the gas holdup, which can be determined with the relation of Achwal and Stepanek (Ramachandran and Chaudari, 1983)

$$\frac{\epsilon_G}{\epsilon_{\text{bed}}} = 2\left(1 + \left(1 + 72.3 v_L^{-0.229} \left(\frac{v_L}{v_G^2} \right)^{0.423} \right)^{1/2} \right)^{-1} \tag{A8}$$

The Péclet group for the radial dispersion coefficient with one phase flow can be determined with (Gunn, 1987)

$$\frac{1}{Pe_A} = \frac{1}{Pe_f} + \frac{\epsilon_{\text{bed}}}{\tau Re_{pL} Sc_A} \tag{A9}$$

in which $\tau = 1.2$ for spheres, and Pe_f is

$$Pe_f = 40 - 29 \exp\left(-\frac{7}{Re_{pL}} \right) \tag{A10}$$

Here Pe_A is the Péclet number of component A ($v_L d_p/\epsilon_{\text{bed}} D_A$). No relation for the dispersion coefficient in a three-phase cocurrent upflow packed-bed reactor has been found. Since the dispersion in this type of reactor will probably be larger, the value obtained with Eq. A9 is used as a minimum value.

The gas–liquid mass transfer in a three-phase packed-bed reactor, $k_{GL}a_B$, can be described with the relation presented by Reiss (1967), and also used by many other authors (Ramachandran and Chaudari, 1983; Winterbottom et al., 1999; Herrmann and Emig, 1998)

$$k_{GL} a_B = 5.48\times10^{-3} (v_L \delta_{LG})^{0.5} \tag{A11}$$

with v_L in $\text{cm}\cdot\text{s}^{-1}$; and δ_{LG} is the frictional pressure gradient per unit height of the column and can be determined with (Turpin and Huntington, 1967) (in dyne/cm^3)

$$\delta_{LG} = \frac{2 f_{LG} v_G^2 \rho_G}{d_{pe}} \tag{A12}$$

The parameter f_{LG} is a two-phase friction factor, and is correlated in terms of the parameter $Z(= Re_G^{1.167}/Re_L^{0.767})$ as

$$\ln f_{LG} = 8 - 1.12 \ln Z - 0.0769(\ln Z)^2 + 0.0152(\ln Z)^3 \quad \text{(A13)}$$

The equivalent diameter of the particles is defined as

$$d_{pe} = \frac{2}{3} \frac{d_p \epsilon_{\text{bed}}}{1 - \epsilon_{\text{bed}}} \quad \text{(A14)}$$

Fiber reactor

The values of $k_{GL}a_B$ are estimated with Eq. A4 for bubble columns for *Re* based on the superficial velocity past the fibers. The use of this relation gives a rough estimation of $k_{GL}a_B$, since the fibers will influence the bubble behavior. The liquid solid mass-transfer coefficient, k_L, can be estimated with a relation given for fiber reactors (Cussler, 1997)

$$Sh_{fA} = 0.8 Re_f^{0.47} Sc_A^{0.33} \quad \text{(A15)}$$

The Re_f number is defined as $\rho_L v_f d_f/\eta_L$, with v_f the velocity past the fibers and Sh_{fA} is based on the diameter of the fiber. Also, this relation gives a rough estimation, because the structure of the fiber rod has a large influence on the form of this equation. Furthermore, the relation is determined for flow normal to the fibers.

Manuscript received Nov. 17, 2001, and revision received Sept. 12, 2002.